Fabian Brinkmann, Vera Erbes, Stefan Weinzierl

Extending the closed form image source model for source directivity

Brinkmann, F.; Erbes, V.; Weinzierl, S. (2018): Extending the closed form image source model for source directivity. In: Fortschritte der Akustik - DAGA 2018 : 44. Jahrestagung für Akustik, 19.-22. März 2018 in München. Berlin: Deutsche Gesellschaft für Akustik e.V., 2018. pp. 1298–1301.

Extending the closed form image source model for source directivity

Fabian Brinkmann[1], Vera Erbes[2], Stefan Weinzierl[1]

fabian.brinkmann@tu-berlin.de, vera.erbes@uni-rostock.de, stefan.weinzierl@tu-berlin.de

[1] *Audio Communication Group, Technical University Berlin, Einsteinufer 17c, 10587 Berlin.*

[2] *Institute of Communications Engineering, University of Rostock, R-Wagner-Str. 31, 18119 Rostock.*

Introduction

The image source model (ISM) is a widespread tool in geometrical room acoustic simulation for the generation of early reflections, which can take into account the source and receiver directivity, as well as the absorption properties of the acoustic environment. A downside of the ISM is the increase in computational effort with increasing image source order caused by costly visibility checks that need to be done separately for each image source [1]. In the special case of a shoebox-shaped, rectangular room, a closed-form ISM exists, without the need for visibility checks [2]. However, the closed-form ISM inherently assumes omnidirectional sources, an assumption that is violated in almost all real-life scenarios. Theoretically, the source directivity affects the sound field at the receiver in the following: i) The spectral shape and energy of direct sound and early reflections changes, which might affect the perceived coloration and source position, and the apparent source width. ii) The direct-to-reverberant energy ratio can be altered, which possibly influences the listener envelopment and perceived duration and strength of the reverberation. iii) The coloration of the late reverberation is influenced by the diffuse field transfer function of the source, i.e. the spatially averaged directivity.

In the current study, the closed-form ISM is extended for the source directivity by exploiting geometrical properties of the room. Sound examples for auralizations from a closed-form ISM combined with a stochastic model for the late reflections are given in the digital appendix [3]. They demonstrate that the approach can be attractive for applications that require perceptually plausible and computationally efficient, rather than physically accurate simulations.

Image source model

According to the ISM, a reflection on a single wall can be simulated by mirroring the source at the wall. This creates a so-called image source, whose distance and angle in relation to a receiver (e.g. a microphone) are identical to the reflected sound path, as shown by the blue image source and reflection path in Fig. 1 (left). The ISM can be applied to arbitrary acoustic environments by successively mirroring the image sources at the room boundaries, which leads to higher-order image sources, where the order denotes how many times the source was mirrored/reflected by a wall. Note that the zeroth order image source is the source itself, and that the term *image source* is used to refer to the source and the image sources in the remainder of this article.

The repeated mirroring of the source results in a cloud of image sources as shown in Fig. 1 (left) for the 2-dimensional slice of a rectangular room. For complex room shapes, not all image sources are visible to the receiver – e.g. due to obstacles inside the room – which requires visibility checks that become computationally expensive with increasing image source order [1]. In the special case of a rectangular room, however, all image sources shown in Fig. 1 are visible, and the corresponding room impulse response h can be calculated by a closed-form expression [2]

$$h(t) = \sum_{\mathbf{u}=0}^{1} \sum_{\mathbf{l}=-\infty}^{\infty} A(\mathbf{u},\mathbf{l}) \cdot \delta(t - \tau(\mathbf{u},\mathbf{l})). \tag{1}$$

Eq. (1) shows that the impulse response consists of a superposition of Dirac pulses $\delta\,/\,\mathrm{Pa{\cdot}m}$ that are weighted by the amplitude $A\,/\,\frac{1}{\mathrm{m}}$, delayed by $\tau\,/\,\mathrm{s}$, and summed across $\mathbf{u} = (u, v, w)$ and $\mathbf{l} = (l, m, n)$. Accordingly, a sum in (1) represents a triple sum, e.g.

$$\sum_{\mathbf{u}=0}^{1} = \sum_{u=0}^{1}\sum_{v=0}^{1}\sum_{w=0}^{1}. \tag{2}$$

The notation follows Lehmann and Johansson [4], and a comprehensive re-formulation of the derivation can be found in the Appendix [3]. $h\,/\,\mathrm{Pa}$ is defined for a room in the first octant of a three-dimensional Cartesian coordinate system with one corner at the origin (cf. Fig. 1). The room size $\mathbf{L}\,/\,\mathrm{m}$, source position $\mathbf{s}\,/\,\mathrm{m}$, and receiver positions $\mathbf{r}\,/\,\mathrm{m}$ are given by

$$\mathbf{L} = \begin{bmatrix} L_x \\ L_y \\ L_z \end{bmatrix}, \quad \mathbf{s} = \begin{bmatrix} s_x \\ s_y \\ s_z \end{bmatrix}, \text{ and } \quad \mathbf{r} = \begin{bmatrix} r_x \\ r_y \\ r_z \end{bmatrix}. \tag{3}$$

The delay τ can be calculated from the distance $d\,/\,\mathrm{m}$ between an image source and the receiver divided by the speed of sound $c\,/\,\frac{\mathrm{m}}{\mathrm{s}}$

$$\tau(\mathbf{u},\mathbf{l}) = d(\mathbf{u},\mathbf{l})/c, \tag{4}$$

and d can be calculated from the position of the image source relative to the receiver $\hat{\mathbf{p}} = [\hat{p}_x\ \hat{p}_y\ \hat{p}_z]^{\mathrm{T}}$

$$d(\mathbf{u},\mathbf{l}) = \sqrt{\hat{p}_x^2 + \hat{p}_y^2 + \hat{p}_z^2}, \tag{5}$$

with

$$\hat{\mathbf{p}} = \begin{bmatrix} (1-2\,u\,)s_x \ +\ 2\ l\ L_x \ -\ r_x \\ (1-2\,v\,)s_y \ +\ 2m\,L_y \ -\ r_y \\ (1-2\,w)s_z \ +\ 2\,n\,L_z \ -\ r_z \end{bmatrix}. \tag{6}$$

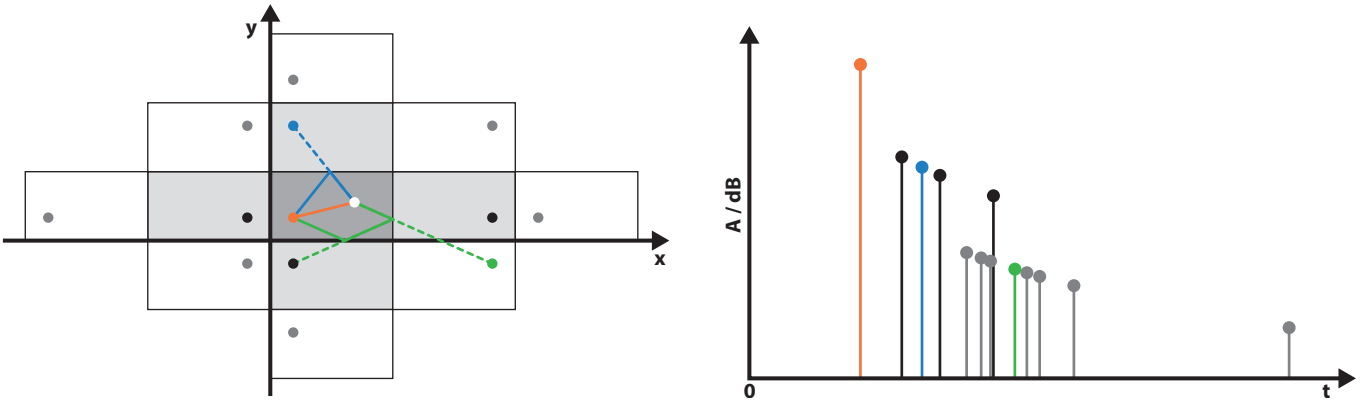

Figure 1: Left: Image sources of a rectangular room (restricted to the x/y-plane). Zeroth, first, and second order image sources are given by orange, black, and gray dots, respectively; the direct sound path and examples for first and second order reflection paths are given by orange, blue, and green lines, respectively. Right: Corresponding room impulse response.

Note that Eq. (6) differs from the original work of Allen and Berkley [2], and was adjusted to correctly reflect $\hat{\mathbf{p}}$ (see section *Image source position* below). Moreover, the absolute image source position is now given by

$$\mathbf{p} = \hat{\mathbf{p}} + \mathbf{r}. \tag{7}$$

The amplitude A is a combination of energy losses caused by wall reflections and the path distance

$$A(\mathbf{u}, \mathbf{l}) = \frac{\beta_{x,1}^{|l-u|}\beta_{x,2}^{|l|}\ \beta_{y,1}^{|m-v|}\beta_{y,2}^{|m|}\ \beta_{z,1}^{|n-w|}\beta_{z,2}^{|n|}}{4\pi d(\mathbf{u}, \mathbf{l})}, \tag{8}$$

with the wall reflection coefficients $\beta_{\mathbf{x},i}^{|k|}$. The subscript $x/y/z$ denotes the coefficient for walls with constant $x/y/z$-coordinates, where $i = 1$ is the wall that is closer to the origin of coordinates. The exponent $|k|$ gives the number of times that an image source was reflected at the corresponding wall - which will be used later to obtain the source exit angles. Moreover, the image source order can be obtained by summing all $|k|$ in Eq. (8). The reflection coefficient is related to the more commonly used absorption coefficient α by

$$\beta = \pm\sqrt{1-\alpha}, \tag{9}$$

whereby $\beta = +\sqrt{\cdot}$ refers to a sound hard reflection on a rigid boundary without any phase shift, and $\beta = -\sqrt{\cdot}$ to a sound soft reflection with a 180° phase shift.

Image source position

The closed-form image source model for rectangular rooms with rigid boundaries was derived from the corresponding 3D wave equation, and thus is a physically correct description of the sound field inside this room. However, Allen and Berkley heuristically derived the dependency of the image source amplitude on the reflection coefficients described in Eq. (8). Strictly spoken, this part of the image source model is physically incorrect, but is widely accepted for moderately damped rooms ($|\beta| \gtrsim 0.7 \Rightarrow \alpha \lesssim 0.5$), and source/receiver positions that are not close to the wall [2].

Unfortunately, the heuristically derived part of the original model contains an error in the description of the relative image source position (Eq. (6, 10, 11) in [2], originally termed $\mathbf{R}_p + \mathbf{R}_\mathbf{r}$). The x-component is given by

$$\hat{p}_{x,\mathrm{AB79}} = (2u-1)r_x + 2lL_x + s_x. \tag{10}$$

The error becomes obvious by the example of the one dimensional image source model given in Fig. 2, where the relative position of *image a* is incorrect for Eq. (10) given by Allen and Berkley – the correct position is given by Eq. (6). Since Allen and Berkley applied Eq. (10) only to obtain the distance between the image source and the receiver as given in Eq. (5), sign errors as occurring for *image b* in Fig. 2 did not affect their results. However, the original formulation cannot be used to calculate the absolute images source position $\mathbf{p}$. It should be noted that the formulation of Allen and Berkley leads to the same absolute values, i.e., distances between image sources and receivers, only the order in which they are calculated is different and produces errors if considering non-rigid walls as some image sources are associated with wrong reflection coefficients.

In conclusion, Eq. (6) and (7) contain the correct image source positions. They are similar to Lehmann and Johansson [4] who used the opposite sign without mentioning the error of Allen and Berkley.

Extension for source directivity

Originally, the ISM does not account for source nor receiver directivity. For this purpose, the exit and incidence angles under which the reflection paths leave the source $\angle_s(\mathbf{u}, \mathbf{l}) = [\varphi_s, \vartheta_s]$ and hit the receiver $\angle_r(\mathbf{u}, \mathbf{l}) = [\varphi_r, \vartheta_r]$ must be known. The latter can simply be calculated from the relative position $\hat{\mathbf{p}}$

$$\varphi_r = \mathrm{arctan2}\left(\frac{\hat{p}_y}{\hat{p}_x}\right), \text{ and } \vartheta_r = \arcsin\left(\frac{\hat{p}_z}{d}\right), \tag{11}$$

where the azimuth φ denotes the counterclockwise angle in the x/y-plane ($\varphi = 0°$ in positive x-direction, and $\varphi = 90°$ in positive y-direction), and the elevation ϑ the

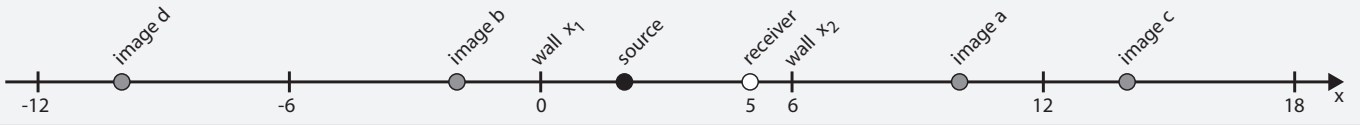

p_x	-10 (-10)	-2 (12)	2 (2)	10 (24)	14 (14)
$\hat{p}_x$	-15 (-15)	-7 (7)	-3 (-3)	5 (19)	9 (9)
$[u,l]$	[0,-1]	[1,0]	[0,0]	[1,1]	[0,1]
$\lvert l-u\rvert$	1	1	0	0	1
$\lvert l\rvert$	1	0	0	1	1

Figure 2: Second-order one-dimensional image source model for the example of $s_x = 2$, $r_x = 5$, and $L_x = 6$. Source and receiver are denoted by the black and white dot; image sources by grey dots. p_x and $\hat{p}_x$ give the absolute and relative image source positions; values in brackets are the positions according to [2, Eq. (6, 10, 11)]. $[u, l]$ gives the values for u and l according to Eq. (1); $|l - u|$ and $|l|$ denote how many times an image sources was reflected by wall x_1 and x_2, respectively (cf. Eq. 8).

angle between the x/y-plane and the z-axis ($\vartheta = 0°$ in the x/y-plane, and $\vartheta = \pm 90°$ in positive and negative z-direction, respectively). $\hat{\mathbf{p}}$ could also be seen as a vector pointing from the receiver to the direction of the image source. An example for the vector interpretation and the calculation of $\angle_r$ is given in Fig. 3.

The usual way to obtain the source exit angles is to perform a visibility check for each image source, by tracing back the reflection path from the receiver to the source [1]. In this iterative procedure, it is checked whether the line between the n^{th} order image source and receiver intersects with the wall by which it was reflected at last. If the intersection exists, it is checked whether the line between the intersection and the $(n\text{-}1)^{th}$ order image source intersects with the wall that corresponds to the current reflection. This procedure is repeated until source is reached, and is aborted if an intersection does not exist. In this case, the image source is not visible to the receiver and can be discarded. For the closed-form model of the rectangular room, however, all image sources calculated by Eq. (1) and shown in Fig. 1 exist, which makes the visibility check obsolete. Please note, that it would still be needed if mirroring the source *by hand*, because two versions of the green image source in Fig. 1 would exist (one first mirrored at wall x_2, and one first mirrored at wall y_1). If using the closed form, tracing the reflection paths is only necessary to obtain the order in which an image source was reflected by the walls. Without this, it is unknown whether the green image source in Fig. 1 was first reflected by wall x_2 and afterwards by wall y_1, or the other way around.

However, due to the geometry of the rectangular room, the source exit angle $\angle_s$ can be obtained in a simple and efficient manner: Because the walls are parallel to the axes of the coordinate system, and orthogonal to each other, each reflection only affects either the x, y, or z coordinate of the ray's propagation path, e.g., if a ray hits a wall that is parallel to the y-axis (reflection coefficients $\beta_{x,i}$) only its x-coordinate is mirrored. As a consequence, i) the order in which a ray hits the walls does not affect the source exit angle, and ii) the direction of propagation stays the same if the number of reflections on walls with constant x, y, and z coordinates is even. Thus, a vector pointing from the source to the first point of reflection

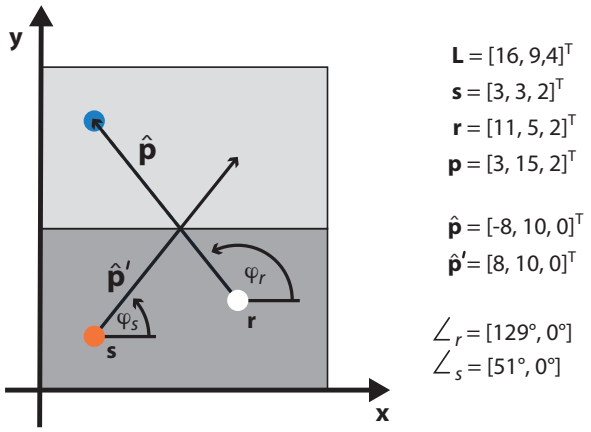

Figure 3: An example of the vector interpretation of $\hat{\mathbf{p}}$ and $\hat{\mathbf{p}}'$, and calculating the exit and incidence angles according to Eq. (11)–(13). The image source was reflected once at wall y_2, and $\hat{\mathbf{p}}'$ was thus obtained for $m = v = 1$ and $l = n = u = w = 0$. Color coding of image sources and receiver according to Fig. 1; $\angle = [\varphi, \vartheta]$.

after the ray left the source can be calculated by

$$\hat{\mathbf{p}}' = - \begin{bmatrix} \hat{p}_x \ (-1)^{|l-u|+|l|} \\ \hat{p}_y \ (-1)^{|m-v|+|m|} \\ \hat{p}_z \ (-1)^{|n-w|+|n|} \end{bmatrix} . \tag{12}$$

In this context, $-\hat{\mathbf{p}}$ can be interpreted as the position of the receiver in relation to the image source, or as a vector pointing from the image source towards the receiver. Eq. (12) takes $-\hat{\mathbf{p}}$ and mirrors its x, y, and z coordinates in case an image source was reflected an odd number of times at walls with constant x, y, and z coordinates. This is denoted by the superscript, e.g., $|l - u| + |u|$ for the walls with constant x-coordinates (cf. Eq. (8), and Fig. 3). The source exit angle can now be calculated in analogy to Eq. (11)

$$\varphi_s = \operatorname{arctan2}\left(\frac{\hat{p}'_y}{\hat{p}'_x}\right), \text{ and } \vartheta_r = \arcsin\left(\frac{\hat{p}'_z}{d}\right). \tag{13}$$

The directivities can now be included in the impulse response calculation by convolution of each pulse $A \cdot \delta(\cdot)$ with the impulse responses of source and receiver (S and

R) at the exit and incident angles

$$h_d(t) = \sum_{\mathbf{u}=0}^{1} \sum_{\mathbf{l}=-\infty}^{\infty} [A(\mathbf{u},\mathbf{l}) \cdot \delta(t - \tau(\mathbf{u},\mathbf{l}))] * S(t, \angle_s(\mathbf{u},\mathbf{l})) * R(t, \angle_r(\mathbf{u},\mathbf{l})). \quad (14)$$

Discussion and conclusion

Despite the variety of room acoustic modelling algorithms that are available for arbitrarily shaped rooms [5, 6], the suggested closed-form image source model for rectangular rooms is still appealing in case of limited computational resources and if aiming at plausible acoustics scenes, rather than at physical correctness. Moreover, the simplicity of the suggested model and the extension for source directivity suggested in the current study, make it easy to implement. It is thus suitable for use in research, where open software is often preferred to foster reproducibility [7]. So far, only frequency-independent reflection factors β were considered, but an extension to frequency-dependent and even complex-valued factors can be achieved by evaluating Eq. (8) at different frequencies. As a consequence, the influence of the reflections could be considered by means of an impulse response $A(t - \tau(\mathbf{u},\mathbf{l}),\mathbf{u},\mathbf{l})$ with a phase behaviour according to the complex β values, or an artificial minimum/linear phase. For the case of complex values, Aretz *et al.* [8] showed that the physically correct modal behaviour of a moderately damped, rectangular room can be computed with the image source model up to one octave above the Schröder frequency. So far, air attenuation is not included in Eq. (8), but could be considered following ISO 9613-1 [9].

The purely specular reflections produced by the image source model become physically incorrect with increasing image source order. For this reason, the image source model is commonly used for calculating early reflections only, and is combined with a stochastic model for the late reverberation [1, 5]. Three examples for such hybrid rectangular room models are McRoomSim [10], RAZR [11], and TASCAR [12], that are intended to provide acoustic simulations for spherical microphone array development and research in hearing aid design. RAZR and TASCAR employ feedback delay networks to model the late reverberation and do not include the source directivity. McRoomSim uses diffuse rain for late reverberation and is capable of simulating the source directivity, however, this is done by the computationally more demanding backwards-tracing of the image source reflection paths.

Appendix

The digital appendix contains a detailed re-formulation of the derivation of the closed-form image source model for rectangular rooms according to [2, Appendix A], and auralizations using an omnidirectional and a directional source that can be compared against a measured counterpart [3]. The auralizations were obtained with the suggested image source model in combination with a stochastic reverb based on decaying noise [13]. The model is part of AKtools, and intended for educational purposes [14].

References

[1] M. Vorländer, *Auralization. Fundamentals of acoustics, modelling, simulation, algorithms and acoustic virtual reality*, 1st ed. Berlin, Heidelberg, Germany: Springer, 2008.

[2] J. B. Allen and D. A. Berkley, "Image method for efficiently simulating small-room acoustics," *J. Acoust. Soc. Am.*, vol. 65, no. 4, pp. 943–950, Apr. 1979.

[3] V. Erbes and F. Brinkmann, "Extending the closed form image source model for source directivity (Digital appendix)," https://dx.doi.org/10.14279/depositonce-6724, Mar. 2018.

[4] E. A. Lehmann and A. M. Johansson, "Prediction of energy decay in room impulse responses simulated with an image-source model," *J. Acoust. Soc. Am.*, vol. 124, no. 1, pp. 269–277, Jul. 2008.

[5] L. Savioja and U. P. Svensson, "Overview of geometrical room acoustic modeling techniques," *J. Acoust. Soc. Am.*, vol. 138, no. 2, pp. 708–730, Aug. 2015.

[6] V. Välimäki, J. Parker, L. Savioja, J. O. Smith, and J. Abel, "More than 50 years of artificial reverberation," in *60th In. AES Conf. DREAMS (Dereverberation and Reverberation of Audio, Music, and Speech)*, Leuven, Belgium, Feb. 2016.

[7] P. Vandewalle, J. Kovačević, and M. Vetterli, "Reproducible research in signal processing – what, why, and how," *IEEE Signal Processing Magazine*, vol. 26, no. 3, pp. 37–46, Apr. 2009.

[8] M. Aretz, P. Dietrich, and M. Vorländer, "Application of the mirror source method for low frequency sound prediction in rectangular rooms," *Acta Acust. united Ac.*, vol. 100, no. 2, pp. 306–319, Mar./Apr. 2014.

[9] ISO 9613-1, *Attenuation of sound during propagation outdoors. Part 1: Calculation of the absorption of sound by the atmosphere.* Geneva, Switzerland: International Organization for Standards, 1993.

[10] A. Wabnitz, N. Epain, C. Jin, and A. van Schaik, "Room acoustics simulation for multichannel microphone arrays," in *Int. Symp. on Room Acoustics (ISRA)*, Melbourne, Australia, Aug. 2010.

[11] T. Wendt, S. van de Par, and S. D. Ewert, "A computationally-efficient and perceptually-plausible algorithm for binaural room impulse response simulation," *J. Audio Eng. Soc*, vol. 62, no. 11, pp. 748 – 766, 2014.

[12] G. Grimm, J. Luberadzka, and V. Hohmann, "Virtual acoustic environments for comprehensive evaluation of model-based hearing devices," *Int. J. Audiology*, 2016.

[13] C. Borß and R. Martin, "An improved parametric model for perception-based design of virtual acoustics," in *AES 35th International Conference*, London, UK, Feb. 2009.

[14] F. Brinkmann and S. Weinzierl, "AKtools – An open software toolbox for signal acquisition, processing, and inspection in acoustics," in *142nd AES Convention, Convention e-Brief 309*, Berlin, Germany, May 2017.